Melting/freezing behavior of a fluid confined in porous glasses and MCM-41: Dielectric spectroscopy and molecular simulation

Malgorzata Sliwinska-Bartkowiak, Grazyna Dudziak, Roman Sikorski, and Roman Gras
Instytut Fizyki, Uniwersytet im Adama Mickiewicza, Umultowska 85, 61-614 Poznan, Poland

Ravi Radhakrishnan and Keith E. Gubbins
North Carolina State University, 113 Riddick Labs, Raleigh, North Carolina 27695-7905

(Received 1 August 2000; accepted 6 October 2000)

We report both experimental measurements and molecular simulations of the melting and freezing behavior of fluids in nanoporous media. The experimental studies are for nitrobenzene in the silica-based pores of controlled pore glass, Vycor, and MCM-41. Dielectric relaxation spectroscopy is used to determine melting points and the orientational relaxation times of the nitrobenzene molecules in the bulk and the confined phase. Monte Carlo simulations, together with a bond orientational order parameter method, are used to determine the melting point and fluid structure inside cylindrical pores modeled on silica. Qualitative comparison between experiment and simulation are made for the shift in the freezing temperatures and the structure of confined phases. From both the experiments and the simulations, it is found that the confined fluid freezes into a single crystalline structure for average pore diameters greater than 20σ, where σ is the diameter of the fluid molecule. For average pore sizes between 20σ and 15σ, part of the confined fluid freezes into a frustrated crystal structure with the rest forming an amorphous region. For pore sizes smaller than 15σ, even the partial crystallization did not occur. Our measurements and calculations show clear evidence of a novel intermediate ''contact layer'' phase lying between liquid and crystal; the contact layer is the confined molecular layer adjacent to the pore wall and experiences a deeper fluid–wall potential energy compared to the inner layers. We also find evidence of a liquid to ''hexatic'' transition in the quasi-two-dimensional contact layer at high temperatures. [DOI: 10.1063/1.1329343]

I. INTRODUCTION

There have been numerous experimental studies on freezing of simple fluids in silica based pores.[1–16] Freezing of oxygen in sol–gel glasses was studied by Warnock *et al.*[1] by a subpicosecond optical technique; the freezing temperature in the confined system was always depressed as compared to the bulk; the shift was larger for smaller pores, and as large as 10 K for the smallest (20 nm) pore. Unruh *et al.*[7] examined the melting behavior of indium metal in porous silica glasses by differential scanning calorimetry (DSC) measurements, and reported a large depression in melting point due to confinement. The simplest way to understand the freezing point shift is through the Gibbs–Thomson equation. This determines the freezing temperature, T_f, as the point at which the chemical potential of the solid core inside the pore equals that of the surrounding fluid (see, e.g., Evans and Marconi[17]). However, this type of classical thermodynamic argument breaks down for small pores due to inhomogeneity and finite size effects. Unruh *et al.*,[7] Molz *et al.*,[6] and Sliwinska-Bartkowiak *et al.*,[16] reported latent heat measurements λ_{fp}, using DSC in the confined systems. The magnitude of λ_{fp} in the above studies was much less than the latent heat in the bulk material. The difference was attributed to the premise that the confined crystalline phase may not be homogeneous, i.e., there may be amorphous regions coexisting with crystalline regions. Such speculations can only be tested if the fluid structure of the confined phases are studied, in addition to thermodynamic properties such as freezing points and latent heats.

There have been experimental reports that investigated the structure of the confined phases through NMR and x-ray diffraction techniques. Overloop and Van Gervan[14] studied freezing of water in porous silica using NMR, and they suggest that in the confined solid phase up to 3 molecular layers adjacent to the pore wall (which they term ''bound water'') have a structure that is different from the crystal phase and from that of the free liquid. The rest of the water molecules in the pore interior were in the form of cubic ice (I_c) and the freezing temperatures were consistent with the Gibbs–Thomson equation. Morishige and Nabuoka[12] used x-ray diffraction to study water in siliceous MCM-41 having a range of pore sizes, and also confirmed the existence of a disordered layer of water molecules near the pore wall, with the inner region being the I_c phase. Morishige and Kawano[13] also studied water in Vycor glass and found evidence for both the cubic I_c phase as well as the ordinary hexagonal (I_h) phase. Baker and co-workers[18] studied the nucleation of ice in sol–gel silicas and MCM-41 and found that the crystal structure depends strongly on the conditions and nature of the porous material, showing characteristics of both I_h and I_c forms. Morishige and Kawano[13] have reviewed other experimental studies of the freezing/melting behavior of water in porous silicas and glasses.

In a recent study, Booth and Strange[15] examined the melting of cyclohexane in porous silica using the NMR technique. The melting temperature was below the bulk melting point, and in the confined solid phase there were two distinct components of the transverse relaxation time. The short component (15–30 μs, comparable to the crystal phase in the bulk) was attributed to the crystal phase in the interior of the pore, and the long component was attributed to a liquidlike contact layer (the layer adjacent to the pore walls). Further lowering of temperature led to the freezing of the surface (contact) layer as well.

Sliwinska-Bartkowiak and co-workers[16] attempted to characterize the melting/freezing transition for a dipolar fluid, nitrobenzene confined in controlled pore glass of different pore sizes, using DSC and dielectric relaxation spectroscopy (DS). The depression in the melting temperature followed the Gibbs–Thomson equation for pore diameters larger than 7.5 nm; however, significant deviation was observed for a pore width of 5 nm. The results from both experiments were in good agreement. The authors also made a quantitative estimate of the rotational relaxation time in the fluid and crystal phases by fitting the measured complex relative permittivity, $\kappa^* = \kappa_r(\omega) - i\kappa_i(\omega)$, to the Debye dispersion equation. In addition to the liquid and crystal phase relaxation, a third relaxation component was observed that supported the existence of a contact layer with dynamic properties that were liquidlike but different from that of the inner layers; in particular, the rotational relaxation times of molecules in the contact layer were about four orders of magnitude slower than molecules in the capillary condensed phase. Slower dynamics of molecules in the contact layer were also reported by Takahara *et al.*,[19] in a neutron scattering study of water confined in MCM-41.

Sliwinska-Bartkowiak *et al.*[20] found evidence of a prefreezing transition in nitrobenzene confined in a 25 nm controlled pore glass (CPG) material that occurs before the confined fluid freezes into a single crystalline structure. The prefreezing produces an intermediate phase, which we term the ''contact layer phase,'' that is characterized by a positionally disordered contact layer but crystalline inner layers. For the system of nitrobenzene in CPG, the contact layer phase appears to be metastable, because the melting occurs in a single step. This was also theoretically established by a study of Landau free energy surfaces using molecular simulation.[20] Recently, Morishige and Kawano[21] found evidence of such a prefreezing transition for methanol confined in MCM-41, using x-ray diffraction measurements. In a separate simulation study, Radhakrishnan *et al.*[22] examined the thermodynamic stability of the contact layer phase as a function of the relative strength of the fluid–wall interaction to the fluid–fluid interaction. The authors concluded that the contact layer phase is metastable for repulsive and weakly attractive pore walls, and is a thermodynamically stable phase for more strongly attracting pore walls.

The effect of confinement on the triple point of CO_2 was examined by Duffy *et al.*[8] using positronium anihilation spectroscopy. The authors found that the confinement of CO_2 in Vycor glass shifts the liquid–solid transition to a considerably lower, and the gas–liquid transition to a considerably higher temperature, than in the bulk. The triple point is reduced both in pressure and temperature from that of the bulk. Recently, Morishige and Kawano[23] employed x-ray diffraction to study freezing of Kr in MCM-41 under isothermal conditions, by varying the pressure, and found that the confined triple point is not a single state point in the $P-T$ diagram, but a region in the $P-T$ plane. The authors attributed the diffuse triple point region for the confined system to heterogeneity of pore sizes, but speculated that the diffuse triple point region is due to coexistence of molecular clusters of different phases. Brown *et al.*[24] reported studies of the microscopic structure of confined solid CO_2 adsorbed in porous Vycor glass using x-ray diffraction. Their study concluded that the confined CO_2 solidifies into crystallites, with a structure that is consistent with the Pa*3* structure (a fcc lattice with molecules oriented along the diagonals of the cubic lattice) of bulk CO_2. The average crystallite size of the solid phase of the confined CO_2 was comparable to the pore dimensions in Vycor, indicating that the solidification occurs separately in each of the pores. However, a significant amount of disorder was observed in the arrangement of the molecules which could not be accounted for with the Debye–Waller effect.

In view of this large body of experimental evidence for a decrease in the freezing temperature due to confinement, it is tempting to assume that a decrease always occurs. However, in a subsequent molecular simulation study of freezing of simple fluids in slit pores, Miyahara and Gubbins[25] showed that T_f was strongly affected by the strength of the attractive forces between the fluid molecules and the pore walls. For repulsive or weakly attractive potentials, T_f decreased. For nonpolar adsorbates and strongly attracting walls such as carbons, an *increase* in T_f was observed. Moreover, the increase in T_f was predicted to be larger for slit than cylindrical pores.[26] Recently, Radhakrishnan *et al.*[22] computed the global freezing diagram for a Lennard-Jones fluid, and showed the dependence of the freezing temperature on the relative strengths of the fluid–wall to the fluid–fluid attractive interactions. The authors also verified some of the predictions by conducting experimental studies on the freezing of CCl_4 and nitrobenzene in porous silica and activated carbon fibers (ACF).

These experimental and simulation studies show that there is a need to characterize the structure of confined phases when studying freezing. Experimental studies involving x-ray diffraction and NMR methods, and the simulation studies involving free energies, establish the presence of stable inhomogeneous confined phases that bear important consequences for the nature of the phase transition as well as for the shift in the freezing temperatures. Although this effect has been understood in the case of simple fluids freezing in slit shaped pores, the nature of the confined phases in the more complicated cases of subnanometer size cylindrical pores, and highly networked pores such as CPG and Vycor are still unknown. In this paper we study the freezing behavior and fluid structure of confined phases in cylindrical and networked porous systems using dielectric relaxation spectroscopy and molecular simulation.

II. METHODS

The nitrobenzene samples were reagent grade chemicals, and were distilled twice at reduced pressure prior to use in the experiment. Nitrobenzene was further dried over Al_2O_3, centrifuged, and stored in the absence of light to avoid contamination by photochemical reactions. The conductivities of the purified nitrobenzene samples were found to be less than $10^{-10}\,\mathrm{ohm}^{-1}\,\mathrm{m}^{-1}$. The porous silica samples used were the commercially available Controlled Pore Glass (CPG) from CPG Inc., with a pore size distribution of about 5% around the mean pore diameter.[27] Different CPG samples having average pore diameters ranging from 50 nm to 7.5 nm were used. We also studied confinement effects in Vycor glass from Corning Inc., having a mean pore size of 4.5 nm,[28] and a silica-based MCM-41 material with mean pore diameter of 2.8 nm. The pore samples were kept under vacuum prior to and during the introduction of the fluid. The MCM-41 samples were synthesized at A. Mickiewicz University, and were characterized using x-ray diffraction and nitrogen adsorption measurements.[29] The characterization results for MCM-41 showed that these crystalline materials consisted of uniform pores in a hexagonal arrangement with a narrow pore size distribution (dispersion less than 5%).[29]

A. Dielectric relaxation spectroscopy (DS)

The relative permittivity of a medium, $\kappa^* = \kappa_r - i\kappa_i$, is in general a complex quantity whose real part κ_r (also known as the dielectric constant) is associated with the increase in capacitance due to the introduction of the dielectric. The imaginary component κ_i is associated with mechanisms that contribute to energy dissipation in the system, due to viscous damping of the rotational motion of the dipolar molecules in alternating fields. The latter effect is frequency dependent. The experimental setup consisted of a parallel plate capacitor of empty capacitance $C_o = 4.2\,\mathrm{pF}$. The capacitance, C, and the tangent loss, $\tan(\delta)$, of the capacitor filled with nitrobenzene between the plates were measured using a Solartron 1260 gain impedance analyzer, in the frequency range 1 Hz–10 MHz, for various temperatures. For the case of nitrobenzene in porous silica, the sample was introduced between the capacitor plates as a suspension of 200 μm mesh porous silica particles in pure nitrobenzene. The relative permittivity is related to the measured quantities by

$$\kappa_r = \frac{C}{C_o}; \quad \kappa_i = \frac{\tan(\delta)}{\kappa_r}. \tag{1}$$

In Eq. (1), C is the capacitance, C_o is the capacitance without the dielectric, and δ is the angle by which current leads the voltage. Nitrobenzene was confined in porous silica (CPG, Vycor, and MCM-41), of pore widths H ranging from 50 nm down to 2.4 nm at 1 atm. pressure. The freezing temperature for bulk nitrobenzene is 5.6 °C (the liquid freezes to a monoclinic crystal). The complex dielectric permittivity, $\kappa^* = \kappa_r - i\kappa_i$, is measured as a function of temperature and frequency.

For an isolated dipole rotating under an oscillating electric field in a viscous medium, the Debye dispersion relation is derived using classical mechanics,[30]

$$\kappa^* = \kappa_{\infty,r} + \frac{\kappa_{s,r} - \kappa_{\infty,r}}{1 + i\omega\tau}. \tag{2}$$

Here ω is the frequency of the applied potential and τ is the orientational (rotational) relaxation time of a dipolar molecule. The subscript s refers to static permittivity (low frequency limit, when the dipoles have sufficient time to be in phase with the applied field). The subscript ∞ refers to the optical permittivity (high frequency limit) and is a measure of the induced component of the permittivity. Further details of the experimental methods are described elsewhere.[16,31] The dielectric relaxation time was calculated by fitting the dispersion spectrum of the complex permittivity near resonance to the Debye model of orientational relaxation.

B. Differential scanning calorimetry (DSC)

A Perkin–Elmer DSC7 differential scanning calorimeter was used to determine the melting temperatures and latent heats of fusion, by measuring the heat released in the melting of nitrobenzene. The temperature scale of the DSC machine was calibrated using the melting temperature of pure nitrobenzene from the literature. The temperature scanning rates used for the melting and freezing runs varied from 0.2 K/min to 0.5 K/min. The background of each raw DSC spectrum was subtracted, based on a second-order polynomial fit to the measured heat flow away from the signals of interest. The melting temperatures in the bulk and confined systems were determined from the position of the peaks of the heat flow signals, and the latent heats were determined based on the scaled area under these signals. The melting temperature was reproducible to within 0.5 °C for larger pores ($\geqslant 25\,\mathrm{nm}$); uncertainties were larger for the smaller pores. These uncertainties are a result of the width of the DSC peaks, which derives in part from variations in pore size and geometry, and from the existence of metastable states. The latent heats were reproducible to within 5%.

C. Simulation

We performed grand canonical Monte Carlo (GCMC) simulations of Lennard-Jones CCl_4 adsorbed in straight cylindrical pores of different pore diameters. The interaction between the adsorbed fluid molecules is modeled using the Lennard-Jones (12,6) potential with size and energy parameters chosen to describe CCl_4 ($\sigma_{ff} = 0.514\,\mathrm{nm}$, $\epsilon_{ff}/k_B = 366.4\,\mathrm{K}$). The pore walls are modeled as a smooth LJ continuum[32] (the cylindrical equivalent of the ''10-4-3'' Steele potential). The fluid–wall interaction energy parameters corresponding to a silica pore were taken from Gelb and Gubbins.[33]

The simulation runs were performed in the grand canonical ensemble, fixing the chemical potential μ, the volume V of the pore, and the temperature T. The system typically consisted of 600–4000 adsorbed molecules. Periodic boundary conditions were employed in the axial dimension of the pore. The simulation was set up such that insertion, deletion and displacement moves were attempted with equal probability, and the displacement step was adjusted to have a 50% probability of acceptance. Thermodynamic properties were

averaged over 100–1000 million individual Monte Carlo moves. The length of the simulation was adjusted such that a minimum of 50 times the average number of particles in the system would be inserted and deleted during a single simulation run.

The method used to calculate the free energy relies on the calculation of the Landau free energy as a function of an effective bond orientational order parameter Φ, using GCMC simulations. The Landau free energy is defined by[34]

$$\Lambda[\Phi] = -k_B T \ln(P[\Phi]) + \text{constant}, \tag{3}$$

where $P[\Phi]$ is the probability of observing the system having an order parameter value between Φ and $\Phi + \delta\Phi$. The probability distribution function $P[\Phi]$ is calculated in a GCMC simulation by collecting statistics of the number of occurrences of a particular value of Φ in the form of a histogram, with the help of umbrella sampling.[35] For a particular phase, for instance phase A, the grand free energy Ω_A is related to the Landau free energy by

$$\exp(-\beta\Omega_A) = \int_{\Phi_{\min,A}}^{\Phi_{\max,A}} d\Phi \exp(-\beta\Lambda[\Phi]). \tag{4}$$

The grand free energy at a particular temperature is calculated by numerically integrating over the order parameter range ($\Phi_{\min,A}$ to $\Phi_{\max,A}$) that corresponds to the particular phase A under consideration. More complete details of the method for confined systems are given elsewhere.[36–38]

Three dimensional bond orientational order parameters[39] that can differentiate between the isotropic liquid phase and common crystalline lattices are employed. These order parameters are defined as follows: each nearest neighbor bond has a particular orientation in space with respect to a reference axis, which can be described by the spherical coordinates (θ,ϕ). Nearest neighbors were identified as those particles that were less than a cutoff distance r_{nn} away from a given particle. We used a cutoff distance $r_{nn} = 1.3\,\sigma_{ff}$. The global order parameter $\overline{Q}_{lm}$ (Ref. 40) is defined as

$$\overline{Q}_{lm} = \frac{1}{N_b} \sum_{i=1}^{N_b} Y_{lm}(\theta_i, \phi_i), \tag{5}$$

where the index i runs over the total number of nearest neighbor bonds N_b and the Y_{lm}'s denote the spherical harmonics. In order that the order parameter does not depend on the overall orientation of the crystal in the simulation cell, rotationally isotropic combinations of the $\overline{Q}_{lm}$'s are defined as[40]

$$Q_l \equiv \left(\frac{4\pi}{2l+1} \sum_{m=-l}^{+l} |\overline{Q}_{lm}|^2 \right)^{1/2}. \tag{6}$$

We have used $\Phi = Q_6$ as the order parameter for the Landau free energy calculations.

III. EXPERIMENTAL RESULTS

A. Dielectric relaxation

The capacitance C and tangent loss $\tan(\delta)$ were measured as a function of frequency and temperature for bulk nitrobenzene and for nitrobenzene adsorbed in CPG, VYCOR, and MCM-41 materials of different pore sizes, ranging from 50 nm to 2.4 nm, from which the dielectric constant $\kappa_r(T,\omega)$ and the loss factor $\kappa_i(T,\omega)$ were calculated. The dielectric constant is a natural choice of order parameter to study freezing of dipolar liquids, because of the large change in the orientational polarizability between the liquid and solid phases. The melting point can be taken to be the temperature at which there is a large increase in the permittivity, as the solid phase is heated. The measurements of κ_r as a function of T are shown in Fig. 1 for bulk nitrobenzene. There is a sharp increase in κ_r at $T = 5.6\,^\circ\text{C}$, corresponding to the melting point of the pure substance. The spectrum of the complex permittivity (κ_r, κ_i vs ω) is fit to the dispersion relation [Eq. (2)], to determine the dielectric relaxation time τ. The frequency range in this study (100 Hz to 10 MHz) is expected to encompass the resonant frequencies corresponding to the dielectric relaxation in the solid and glass phases. According to Eq. (2), the κ_r function shows a point of inflection and the κ_i function goes through a maximum at the resonant frequency. Therefore, from a spectrum plot of κ_r, κ_i vs $\log_{10}(\omega)$, the relaxation time can be calculated as the reciprocal of the frequency corresponding to a saddle point of the κ_r function or a maximum of the κ_i function. An alternative graphical representation of the Debye dispersion equation is the Cole–Cole diagram,[41] in the complex κ^* plane. The Cole–Cole diagram falls on a semicircle for each relaxation mechanism. From a plot of κ_i vs κ_r, τ is given by the reciprocal of the frequency at which κ_i goes through a maximum.

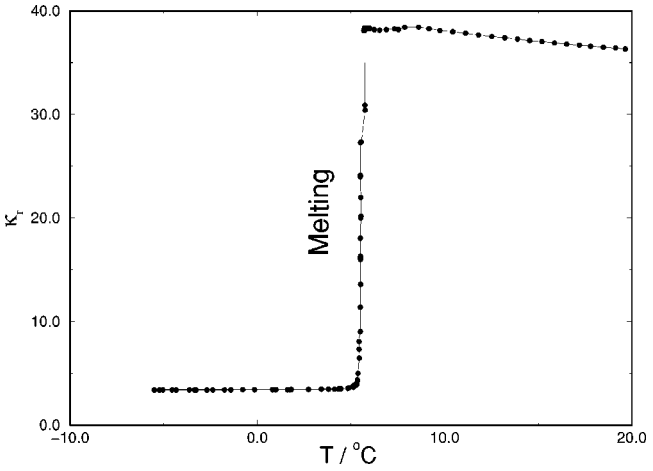

FIG. 1. The behavior of κ_r vs T for bulk nitrobenzene. The sharp increase at 5.6 °C corresponds to bulk melting.

The variation of the relaxation time with temperature for bulk nitrobenzene is shown in Fig. 2, and is obtained from fitting the dispersion spectrum to Eq. (2). The liquid branch of the plot (above 6 °C) has rotational relaxation times of the order of nanoseconds. This branch lies outside the range of our measurements and is reproduced from Ref. 42. The relaxation time shows a sharp increase at the melting temperature and is of the order of 10^{-3} s in the crystal phase.

For nitrobenzene confined in CPG, the sample is introduced between the capacitor plates as a suspension of nitrobenzene-filled CPG particles in pure nitrobenzene.

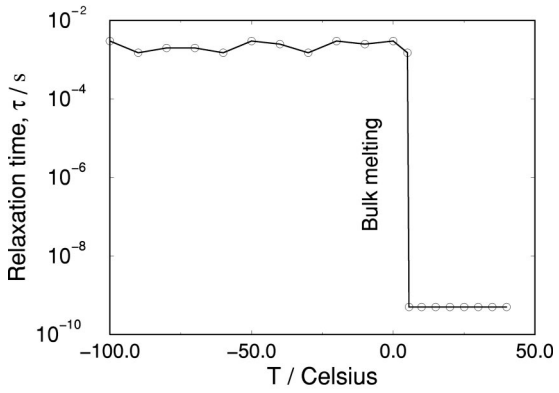

FIG. 2. Relaxation time vs temperature for bulk nitrobenzene. At each temperature τ is estimated by fitting the dispersion spectrum to the Debye dispersion equation.

Therefore, the capacitance measurement yields an effective relative permittivity of the suspension of CPG in pure nitrobenzene. For a CPG sample with average pore diameter of 25 nm, κ_r shows two sudden changes (Fig. 3). The sharp increase at 2 °C is attributed to melting in the pores, while that at 5.6 °C corresponds to the bulk melting. The frequency spectrum at a particular temperature is used to obtain the orientational relaxation times in the different phases of the system as described before. For example, in Figs. 4, and 5 the spectrum plot (κ_r, κ_i vs ω) is shown for nitrobenzene confined in the 25 nm CPG material at two different temperatures. The spectrum in Fig. 4 at 20 °C shows two relaxation mechanisms (as seen by the two inflection points in κ_r) with relaxation times of the order of 10^{-3} s (which we refer to as ''millisecond relaxation'') and 100×10^{-6} s. A similar spectrum at -10 °C (Fig. 5) produces just one relaxation mechanism with a time scale of 10^{-3} s. The corresponding Cole–Cole diagrams are shown in Figs. 6, and 7. The response to each relaxation mechanism falls on a semicircle in the Cole–Cole diagram. Therefore, Fig. 6 confirms the two relaxation mechanisms at the higher temperature (20 °C), and the single relaxation mechanism at the lower temperature (-10 °C) is evident from Fig. 7.

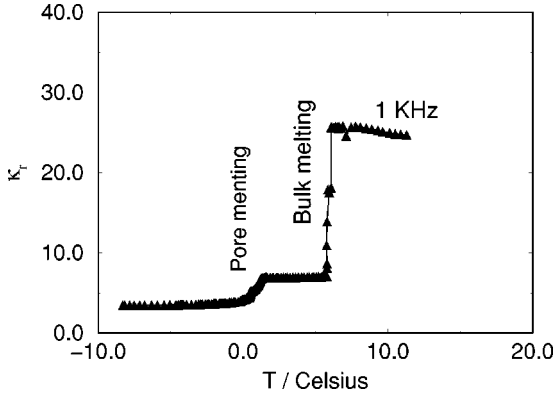

FIG. 3. The behavior of κ_r vs T for nitrobenzene in a CPG material of average pore diameter of 25 nm. The sample is introduced as a suspension of porous glass particles in bulk nitrobenzene. Thus, the signals are for both bulk and confined nitrobenzene.

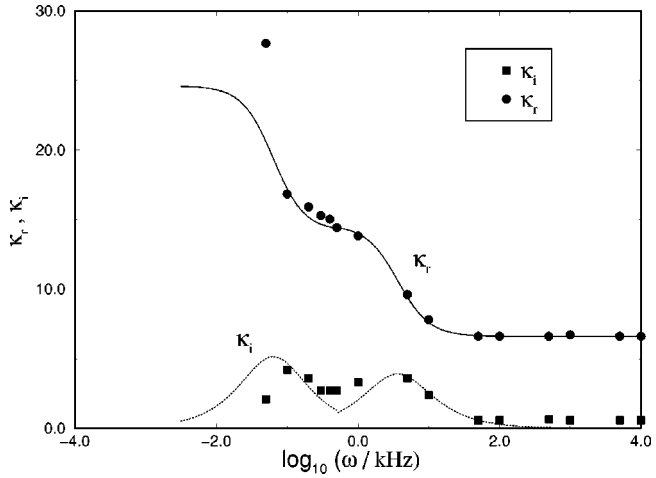

FIG. 4. Spectrum plot for nitrobenzene in a 25 nm pore at 20 °C. The symbols correspond to experimental measurements and the solid and the dashed curves are fits to the real and imaginary parts of Eq. (2), respectively.

B. Maxwell–Wagner effect

The behavior of the relaxation times as a function of temperature for nitrobenzene in CPG of 25 nm pore size are depicted in Fig. 8. For temperatures greater than 2 °C (melting point inside the pores), there are two different relaxations similar to Fig. 4; they manifest themselves as a double inflection behavior in κ_r vs ω, and a double maximum in κ_i vs ω. The longer component of the relaxation that is of the order of 5×10^{-3} s is because of Maxwell–Wagner–Sillars (MWS) polarization. For a heterogeneous system there occurs a relaxation mechanism due to interfacial polarization, when a slightly conducting liquid is enclosed in an insulating material. This effect, MWS polarization,[43] is known to have a relaxation time of the order of 10^{-3} s.[44,45] The CPG and Vycor samples used in this study were dielectrically neutral, in the sense that, in the temperature and frequency range of our measurements, the dielectric loss (proportional to κ_i) of the empty pores was negligible compared to that for the liquid-filled samples. Therefore, there is no background

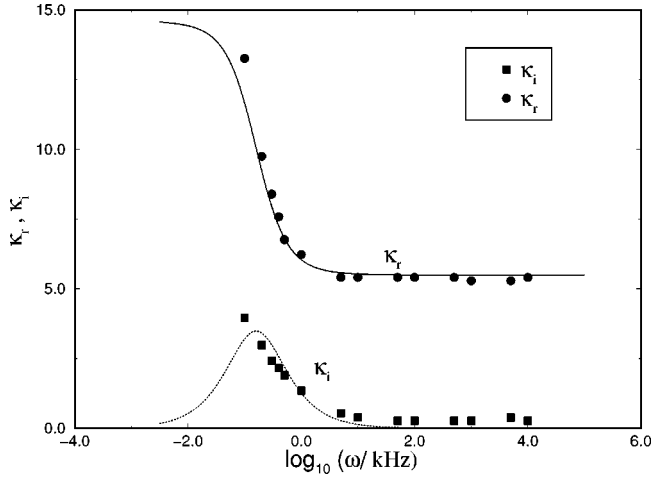

FIG. 5. Spectrum plot for nitrobenzene in a 25 nm pore at -10 °C. The symbols correspond to experimental measurements and the solid and the dashed curves are fits to the real and imaginary parts of Eq. (2), respectively.

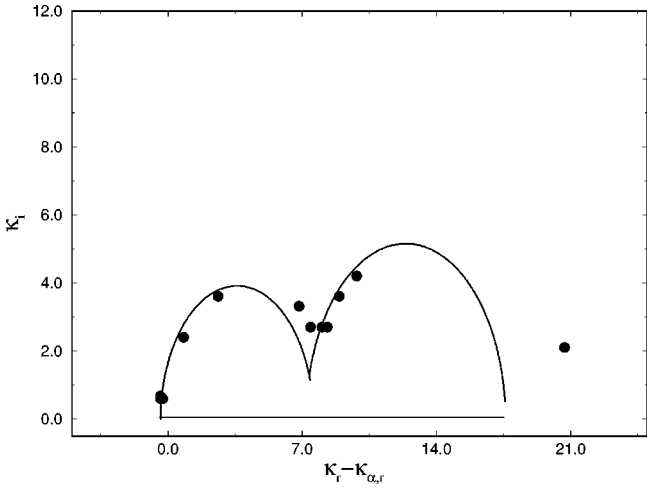

FIG. 6. Representation of the spectrum plots in the form of a Cole–Cole diagram at $T=20\,^{\circ}\mathrm{C}$ for 25 nm CPG.

noise due to the motion of silica molecules. The shorter relaxation component, of the order of 100×10^{-6} s, is too slow to represent the liquid phase relaxation in the pore. However, it is known that for dipolar liquids confined in nanoscale pores, the molecules in the contact layer show a slower dynamics, with a relaxation time of the order of 10^{-5} s.[44–46] Thus, the shorter relaxation component is consistent with such a behavior of the contact layer. The Landau free energy calculation for methane and CCl_4 in graphite,[36,47] and for CCl_4 in silica,[22] and the NMR study by Overloop and Van Gerven[14] dealing with water in porous silica, also support the view that the molecules in the contact layer behave differently than those in the pore interior. Thus, the 100×10^{-6} s branch of the relaxation time that occurs for temperatures above 2 °C (Fig. 8), corresponds to the response of the contact layer. The response of the liquid phase in the bulk and the inner layers of the pore are not accessible in our experiments as subnanosecond relaxation times are not affected by the frequency range we use in our experiments. The disappearance of the 100×10^{-6} s branch of the relaxation time and the appearance of the 10^{-3} s branch at 2 °C, points to

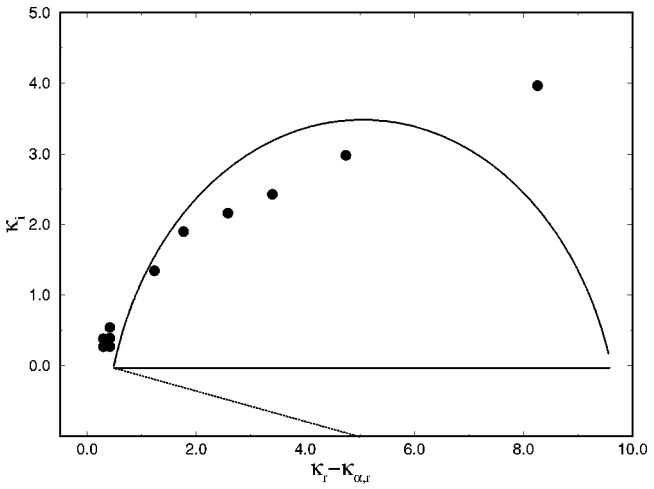

FIG. 7. Representation of the spectrum plots in the form of a Cole–Cole diagram at $T=-10\,^{\circ}\mathrm{C}$ for 25 nm CPG.

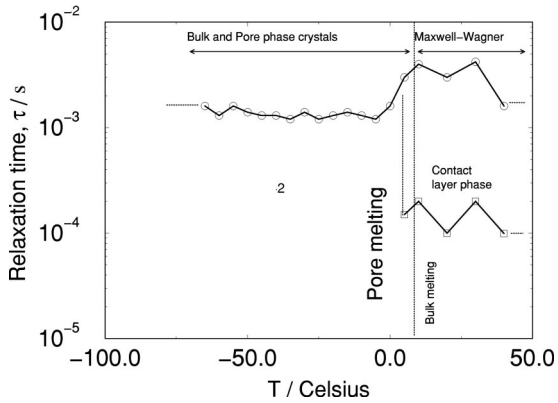

FIG. 8. The behavior of τ vs T for nitrobenzene in a CPG material of average pore diameter of 25 nm. The sample is introduced as a suspension of porous glass particles in bulk nitrobenzene. The signals are for both bulk and confined nitrobenzene.

the freezing of the liquid in the pores. Below this temperature, the millisecond relaxation time (similar to Fig. 5 at $-10\,^{\circ}\mathrm{C}$) corresponds to the crystal phase relaxation in the bulk and in the pore. The MWS effect disappears because the CPG particles are arrested in the crystalline matrix of bulk nitrobenzene, thereby preventing interfacial dispersion. Thus, from Fig. 3 and Fig. 8, the melting temperature of the fluid inside the pore is determined to be 2 °C.

C. Contact layer phase

For fluid molecules such as nitrobenzene that wet the pore walls, the adsorbate molecules in the contact layer next to the pore walls feel a large attractive potential energy due to the combined interactions with all the atoms of the porous material. The density of the adsorbed molecules in the contact layer, is much higher than the bulk liquid density or the average density of the confined fluid phase. In addition, the locus of the surface defining this attractive potential energy is approximately a cylindrical shell, as the pores in CPG, Vycor, and MCM-41 have a cylindrical shape. Such a cylindrical shell is quasi-two-dimensional in nature (a cylindrical shell of radius R and length L, that is cut along a single line parallel to the axis, forms a rectangular two-dimensional plane of dimensions $2\pi R\times L$). Due to the high density of the adsorbed nitrobenzene molecules in the quasi-two-dimensional contact layer, there is a possibility that the contact layer exists as a ''hexatic phase'' with a high degree of orientational ordering. In two-dimensional systems such a hexatic phase lies in between the disordered liquid phase and ordered crystalline phase. The hexatic phase is a manifestation of the fact that, in a continuous symmetry breaking transition such as the freezing transition, the translational symmetry and the rotational symmetry can break at two different temperatures.[48] Thus, in the liquid to hexatic phase transition, the rotational symmetry is broken and in the hexatic to crystalline transition the translational symmetry is broken. According to theory,[49–52] the hexatic phase occurs only for an infinite two-dimensional system, but finite systems such as the contact layer phase can show behavior reminiscent of

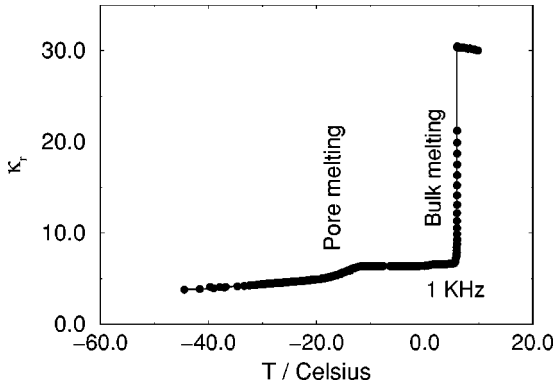

FIG. 9. κ_r vs T for nitrobenzene in CPG with average pore size of 7.5 nm.

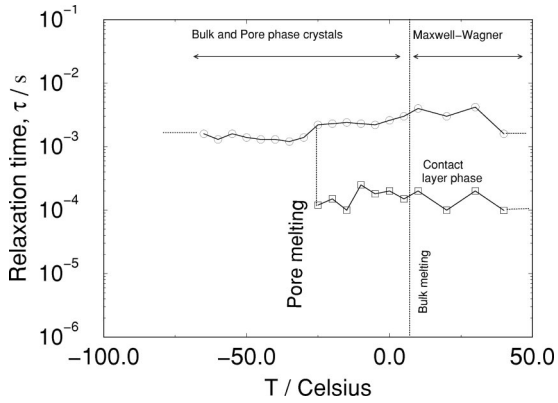

FIG. 10. τ vs T for nitrobenzene in CPG with average pore size of 7.5 nm.

infinite systems. The slower dynamics of the contact layer phase (with τ of the order of 100×10^{-6} s) can be an attribute of its hexatic nature. Such a hexatic phase is predicted by computer simulation for fluids confined in graphitic micropores such as activated carbon fibers, and has been supported by experiments.[22,36,47] For nitrobenzene confined in activated carbon fibers, Radhakrishnan *et al.*[22] found that the nitrobenzene molecules in the hexatic phase have a dielectric relaxation time of the order of 1×10^{-6} s.

Surface heterogeneity can also play a significant role in governing the dynamics of the contact layer. Surface characterization studies of CPG, Vycor, and MCM-41 (Refs. 46, 53, 54) have reported that the silica surface is energetically heterogeneous in such materials. In particular, there is a large concentration of silanol (Si–O–H) on the pore surface, as large as 3 groups per nm^2 in silicious MCM materials.[53] This implies that among the nitrobenzene molecules that are present in the contact layer, a large fraction (as large as 75%) can be weakly hydrogen bonded to the surface silanol groups. The difference in the dielectric relaxation times of the contact layer phase in the ACF micropores ($\tau\sim1\times10^{-6}$ s) and that of the contact layer phase in CPG, Vycor, and MCM-41 ($\tau\sim100\times10^{-6}$ s) is two orders of magnitude. The additional H-bonding with the surface silanol groups in the silica based pores (CPG, Vycor, and MCM-41) can explain the slower dynamics of the contact layer when compared to the ACF micropores, in which H-bonding is absent.

D. Effect of pore-size

In Figs. 9 and 10 are shown κ_r and τ for the freezing of nitrobenzene in a 7.5 nm CPG material. The trends are qualitatively similar to that observed for the 25 nm pore. Figure 9 shows that the increase in κ_r corresponding to the melting of nitrobenzene in the pores is much more rounded and occurs at a lower temperature compared to the bigger pores. From the relaxation time behavior in Fig. 10, we estimate the melting temperature inside the pores to be $-23\,^\circ$C (the temperature below which the 100×10^{-6} s relaxation disappears). The 10^{-3} s branch of the relaxation time in Fig. 10 is divided into three regions. The response in the region, $T>6\,^\circ$C is due to MWS polarization; $-23<T<6\,^\circ$C corresponds to the relaxation of the bulk crystal and $T<-23\,^\circ$C is due to the combined relaxation of the bulk crystal and the crystal inside the pores.

For average pore diameter $H\geqslant7.5$ nm, the behavior of the relaxation time with temperature suggests that the crystalline phase in the pore is a homogeneous phase; i.e., molecules have a single relaxation component throughout the confined crystalline phase. For smaller pores however, e.g., Vycor with $H=4.5$ nm, the behavior is quite different. Figure 11 shows that the increase in κ_r with temperature is more gradual and rounded for the melting of nitrobenzene in the pores. The bulk signal shows the usual sharp increase at $5.6\,^\circ$C and is outside the range of the plot in Fig. 11. In Fig. 12 is plotted the corresponding relaxation times for nitrobenzene melting in Vycor glass. The 100×10^{-6} s branch of the relaxation time shows a sharp increase at $T=-40\,^\circ$C, which can be taken to be the melting temperature inside the pores. The millisecond branch is again divided into three regions, $T>5.6\,^\circ$C (MWS polarization), $-40<T<5.6\,^\circ$C (bulk crystal phase) and $T<-40\,^\circ$C corresponding to the crystalline phase relaxations in the bulk and in the pore. However, there is a new branch of relaxation times of the order of a few hundred nanoseconds which occurs below the melting temperature of nitrobenzene in the pores ($T<-40\,^\circ$C). This

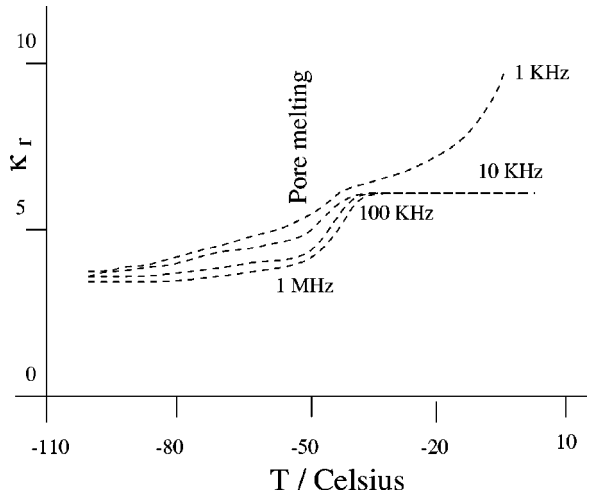

FIG. 11. κ_r vs T for nitrobenzene in Vycor with average pore size of 4.5 nm.

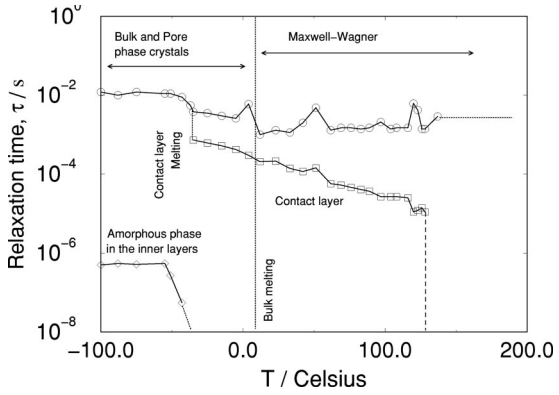

FIG. 12. τ vs T for nitrobenzene in Vycor with average pore size of 4.5 nm.

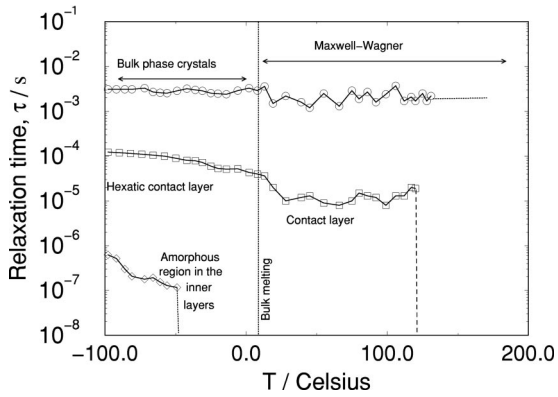

FIG. 14. τ vs T for nitrobenzene in MCM-41 with average pore size of 2.8 nm.

strongly suggests that the confined crystalline phase in not homogeneous, but that there are regions that are glasslike (amorphous), having a relaxation component of the order of a few hundred nanoseconds. Thus for pore diameters as small as 4.5 nm, the confinement poses a serious constraint on the formation of a homogeneous crystalline phase in the pore. The exact structure of the confined crystalline phase cannot be determined from dielectric relaxation spectroscopy experiments alone. One would need to resort to more direct methods, such as x-ray diffraction and molecular simulation, in order to obtain the fluid structure of the inhomogeneous crystalline phase.

In Figs. 13 and 14 the melting behavior of nitrobenzene in a MCM-41 porous material having an average pore diameter of 2.8 nm are shown. The qualitative behavior is different from the behavior in Vycor. The freezing transition at low temperature is absent as the 100×10^{-6} s branch of the relaxation time does not show any discontinuity. Once again there is a branch of relaxation times of the order of a few hundred nanoseconds, suggesting the presence of amorphous regions. We conclude that the pore size of 2.8 nm is too small so that partial crystallization does not occur. The contact layer possibly remains in the orientationally ordered phase, while the inner region undergoes a glass transition. A very similar behavior is observed for the case of nitrobenzene inside an MCM-41 material of pore diameter 2.4 nm. Table I summarizes the melting behavior of nitrobenzene for a range of pore sizes in various silica-based pores. Nitrobenzene freezes to a crystalline structure when confined in pore sizes $H\geqslant 7.5\,\mathrm{nm}$ ($H\geqslant 15\sigma_{ff}$). For a pore size of 4.5 nm, only part of the fluid freezes, with the rest forming an amorphous phase. Morishige and Kawano[55,56] reached similar conclusions in their x-ray diffraction study of freezing of N_2, CO, and Kr in MCM-41 materials of varying pore diameter. For these fluids, the x-ray structure indicated a homogeneous crystalline phase for pore diameters greater than 6 nm ($H\geqslant 16\sigma_{ff}$). For smaller pore sizes, the x-ray diffraction patterns were consistent with a partially crystalline confined phase coexisting with an amorphous phase. For pore sizes smaller than 2.8 nm, the confined fluid does not undergo a freezing transition; however, a glass transition is observed.

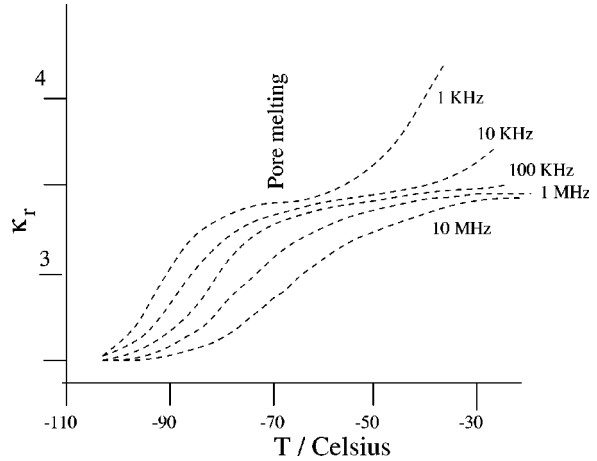

FIG. 13. κ_r vs T for nitrobenzene in MCM-41 with average pore size of 2.8 nm.

E. The hexatic transition

The proposition that the quasi-two-dimensional contact layer may exist as a hexatic phase implies that at higher temperatures, the ''hexatic'' contact layer can undergo a transition to an orientationally disordered, liquidlike contact layer. In Figs. 12 and 14, the disappearance of the 100×10^{-6} s branch of the relaxation time at high temperatures (100 °C), suggests such a transition from a hexatic contact layer phase with a relaxation time $\tau=100\times10^{-6}$ s to a liquidlike contact layer with nanosecond relaxation time. The transition from hexatic to liquid phase is a Kosterlitz–Thouless (KT) type transition,[57,58] and involves a large entropy change. In two dimensions, the specific heat shows a

TABLE I. Freezing temperatures: Experimental measurement.

H/nm	H/σ_{ff}	T/°C	Ordered phase
Bulk	···	5.6	crystal
25 (CPG)	50	2.0	crystal
7.5 (CPG)	15	−25	crystal
4.5 (Vycor)	9	−40	crystal+glass
2.8 (MCM-41, Si)	5.6	−50	glass
2.8 (MCM-41, Al)	5.6	−65	glass
2.4 (MCM-41, Si)	4.8	−65	glass

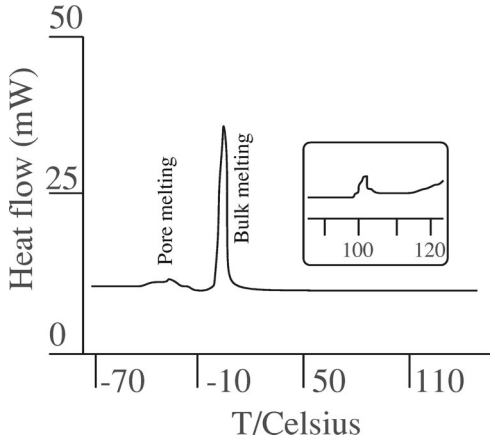

FIG. 15. DSC scan for nitrobenzene confined in Vycor glass. The inset is magnified 100 times compared to the original scan.

nonuniversal peak at the KT transition. We performed DSC measurements for the case of nitrobenzene adsorbed in Vycor and MCM-41 (Figs. 15 and 16). The DSC scan in Fig. 15 shows a large peak at 5.6 °C corresponding to the melting of bulk nitrobenzene. In addition, there is a small peak at lower temperature (-35 °C) corresponding to melting of nitrobenzene confined inside the pores of Vycor. A magnified view of the high temperature region (90–120 °C) shows an additional peak which is consistent with the KT behavior (i.e., hexatic to liquid transition). This peak occurs at a temperature that is well below the capillary condensation transition; capillary condensation occurs above 250 °C for nitrobenzene in Vycor at 1 atm. pressure. Nitrobenzene in MCM-41 (Fig. 16) shows a similar evidence of the hexatic to liquid transition at about 100 °C.

Thus, for nitrobenzene in Vycor and MCM-41 materials, the data suggests that the contact layer phase may exist as a hexatic phase until a temperature of 100 °C, above which it transforms into a liquid phase. This transition could either be a transition between an orientationally ordered phase of dipoles [see cartoon in Fig. 17(a)], to a phase with random orientation of dipoles, or a transition between a phase in which the centers of the molecules (or the nearest neighbor bonds) are orientationally ordered [see cartoon in Fig. 17(b)]

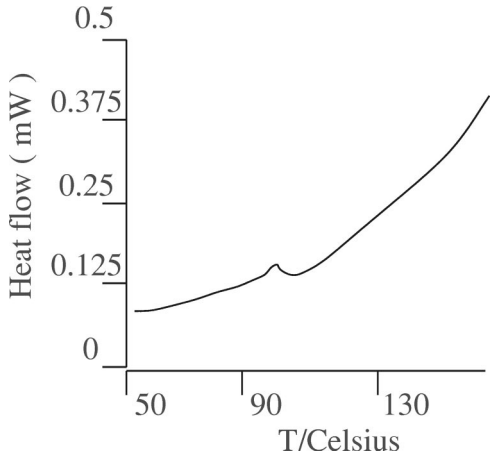

FIG. 16. DSC scan for nitrobenzene confined in MCM-41.

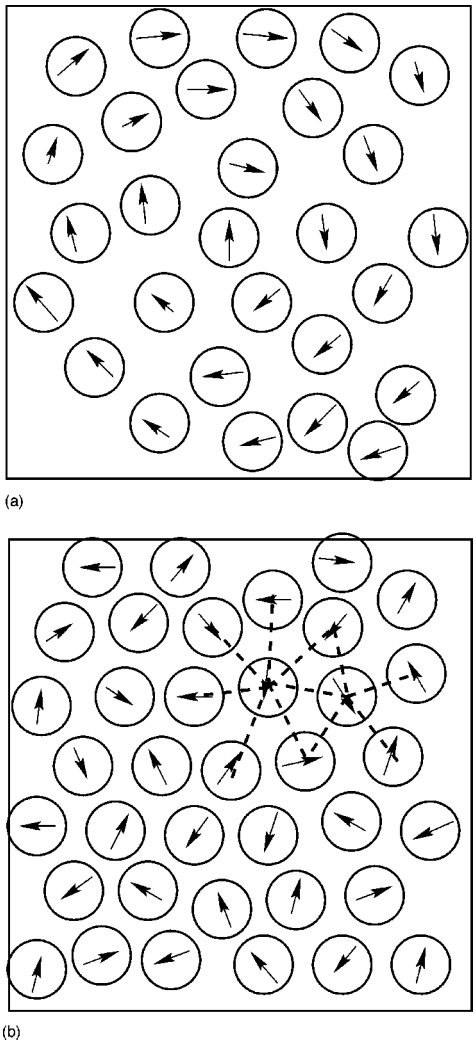

FIG. 17. Cartoon showing the possible hexatic phases in the ''unwrapped,'' quasi-two-dimensional contact layer. (a) Hexatic phase involving dipole orientations; the configuration corresponds to a vortex with its core at the center of the box. (b) Hexatic phase involving the orientation of nearest-neighbor bonds; the nearest neighbor bonds are orientationally ordered; there is a coordination of six nearest neighbors for every molecule, with an occasional five-seven bound pair indicated by the dashed bonds.

to a disordered liquid like phase. Figure 17(a) represents a hexatic phase of dipole orientations (the dipole orientations for a vortex pattern) and Fig. 17(b) represents a hexatic phase of nearest neighbor bonds (bound pairs of five and seven coordinations are found as depicted by the dashed bonds), and a hexatic to liquid transition for both cases is expected to show a peak in the heat capacity. Conclusive evidence on the nature of the transition can only be obtained by careful study of the specific heat and x-ray diffraction, coupled with molecular simulations.

IV. SIMULATION

The molecular simulations were performed for a spherical LJ fluid (with parameters chosen to mimic CCl_4) freezing in smooth silica cylinders of different pore diameters. Qualitative comparison is made with the DS and DSC experiments. Such a simplified model is expected to capture the high temperature hexatic to liquid transition and to elucidate

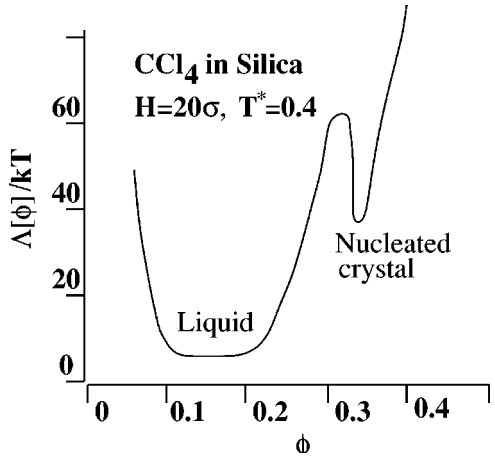

FIG. 18. The Landau free energy as a function of the order parameter, $\Phi = Q_6$, at $T^* = 0.4$ showing two minima. The minimum corresponding to the liquid phase is close to $\Phi = 0$ and the fcc crystalline phase is represented by the minimum centered around $\Phi = 0.35$.

the effect of varying pore diameter on the structure of the confined fluid and crystalline phases. Four different pore diameters ($H = 9\sigma_{ff}$, $12\sigma_{ff}$, $15\sigma_{ff}$, and $20\sigma_{ff}$) were chosen for study. The confined fluid structure was monitored by calculating the local density profile and pair correlation functions and by viewing snapshots of molecular configurations. The freezing temperature was calculated by using the Landau free energy methodology as outlined in Sec. II C. We also calculated the two-dimensional, in-plane pair correlation function $[2D\ g(r)]$ and the two-point orientational correlation functions in the unwrapped contact layer to look for the possibility of a hexatic to liquid transition in the contact layer at high temperatures.

In order to calculate the two-point orientational correlation function, we invoked the hexatic order parameter[49] defined as

$$\Psi_6 = \frac{1}{N_b}\sum_{k=1}^{N_b} \exp(i6\theta_k) = \langle \exp(i6\theta_k) \rangle. \tag{7}$$

Ψ_6 measures the hexagonal bond order in the unwrapped contact layer. Each nearest neighbor bond (as defined in Sec. II C) has a particular orientation in the plane of the unwrapped contact layer, with respect to a reference axis, and is described by the polar coordinate θ. The index k runs over the total number of nearest neighbor bonds, N_b, in the contact layer. We expect $\Psi_6 = 0$ when the contact layer has the structure of a two-dimensional liquid, $\Psi_6 = 1$ in the crystalline phase and $0 < \Psi_6 < 1$ in the orientationally ordered hexatic phase. The two-point orientational correlation function in the unwrapped contact layer is defined as $\langle \Psi_6^*(0)\Psi_6(r) \rangle$. The decay of the $\langle \Psi_6^*(0)\Psi_6(r) \rangle$ function with increasing r is different in liquid, hexatic, and crystalline phases; the correlation function shows an exponential decay in the isotropic liquid phase, algebraic decay ($1/r$ behavior) in the hexatic phase, and is a constant in the crystalline phase. The liquid to hexatic transition temperature in the contact layer is estimated by monitoring the change in behavior of the two-point orientational correlation function with temperature.

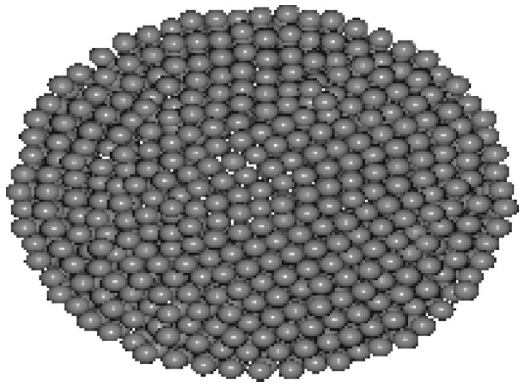

FIG. 19. A snapshot from molecular simulation showing the confined fcc crystalline phase of LJ CCl_4 in a silica cylinder of diameter $20\sigma_{ff}$ at temperature $T^* = 0.38$.

A. Freezing of the confined phase

The Landau free energy function for LJ CCl_4 in a cylindrical silica pore of diameter $20\sigma_{ff}$ at $k_B T/\epsilon_{ff} = 0.4$ is shown in Fig. 18. The order parameter Φ is equal to Q_6 defined in Eq. (6). The minimum centered around $\Phi = 0$ corresponds to a liquidlike phase and that centered around $\Phi = 0.35$ corresponds to a fcc crystalline phase. The grand free energy of the liquid and crystalline phases at $T^* = 0.38$ [calculated using Eq. (4)] are equal; therefore the freezing temperature for this system is $T^* = 0.38$. A snapshot from the simulation of the fcc crystalline phase at $T^* = 0.38$ is shown in Fig. 19. It is evident from the simulations that for a pore diameter of $20\sigma_{ff}$ the fluid freezes into a fcc crystalline phase inside the cylinder. For pore diameters smaller than $20\sigma_{ff}$, the minimum in the landau free energy function corresponding to the fcc crystalline phase did not exist. The pair correlation functions and the snapshots from the molecular simulations strongly indicate a glass transition instead. A snapshot from the simulations for LJ CCl_4 in a cylindrical pore of diameter $H = 12\sigma_{ff}$ is shown in Fig. 20; the temperature corresponds to $T^* = 0.34$ and the snapshot is consistent with the amorphous nature of the confined phase.

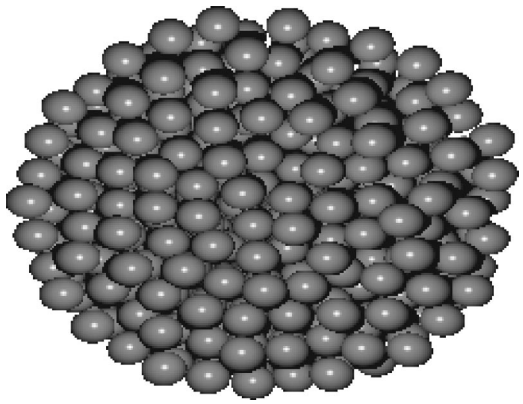

FIG. 20. A snapshot from molecular simulation showing the confined phase of LJ CCl_4 in a silica cylinder of diameter $12\sigma_{ff}$ at temperature, $T^* = 0.34$. The confined phase consists of a hexatic contact layer and an amorphous inner region.

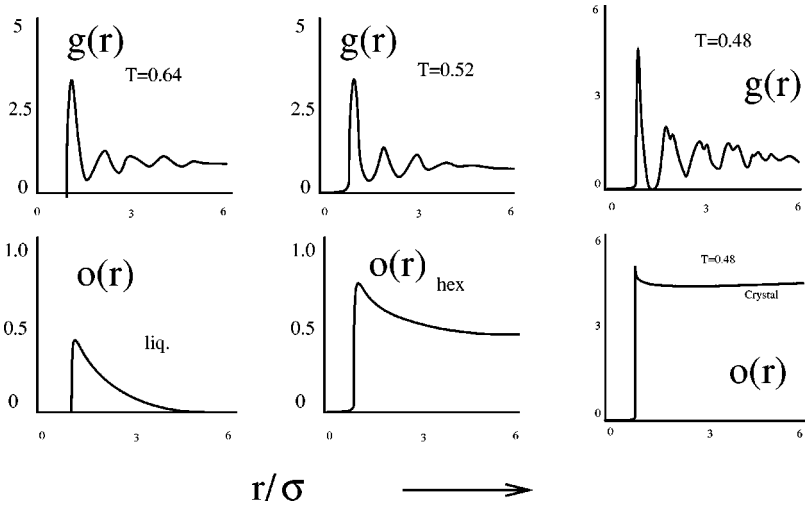

FIG. 21. Two-dimensional, in-plane positional correlation functions $[g(r)]$ and orientational correlation functions $[o(r)=\langle\Psi_6^*(0)\Psi_6(r)\rangle]$ for three different temperatures in the unwrapped contact layer shell. The plots are for LJ CCl_4 in a silica cylinder of diameter $15\sigma_{ff}$, showing the liquid, hexatic and crystalline phases in the contact layer at $T^*=0.64$, $T^*=0.52$, and $T^*=0.48$, respectively.

B. Hexatic transition in the contact layer

The two-dimensional, in-plane pair correlation functions [positional pair correlation function, $g(r)$ and orientational correlation function $\langle\Psi_6^*(0)\Psi_6(r)\rangle$, where $\Psi_6(r)$ is given by Eq. (7)] were monitored as a function of temperature in the unwrapped contact layer shell. The correlation functions for the contact layer shell confined in a cylinder of diameter $15\sigma_{ff}$ are shown in Fig. 21 at three different temperatures. At a high temperature of $T^*=0.64$, the pair correlation is isotropic and the orientational correlation function decays to zero exponentially, suggesting a liquidlike contact layer. As the temperature is lowered to $T^*=0.52$, the pair correlation function is isotropic but displays long range correlations. The orientational correlation function decays algebraically ($1/r$ behavior), which is a clear signature of a hexatic (orientationally ordered) contact layer phase. On further reducing the temperature to $T^*=0.48$, the contact layers freezes to a hexagonal crystal. This is manifested as split peaks in the pair correlation function and no decay in the orientational correlation function. On further lowering the temperature, there is partial crystallization in the inner regions of the confined fluid phase with the rest forming an amorphous phase, as discussed in Sec. IV A. It is clear from the simulations that the hexatic transition in the contact layer is a transition involving nearest neighbor bonds as spherical LJ molecules are orientationally isotropic.

The behavior of the contact layer phase in a smaller cylinder ($H=12\sigma_{ff}$, Fig. 22) is significantly different. At high temperature, $T^*=0.64$, the contact layer correlation functions are typical of the liquid phase, and at $T^*=0.48$, there is a clear signature of a hexatic phase behavior (compare with Fig. 21 at $T^*=0.52$). There is a significant difference in the behavior of the contact layer phase at low temperature. The correlation functions at $T^*=0.38$ indicate that even at such a low temperature, the contact layer does not undergo a freezing transition. This is consistent with the fact that the Landau free energy functions, as well as the pair correlation functions and the snapshots, did not support any evidence of a crystalline or a partially crystalline confined phase for cylinders with diameters smaller than $12\sigma_{ff}$ (see Sec. IV A). The simulation results of the freezing behavior of LJ CCl_4 in silica-based cylinders are summarized in Table II.

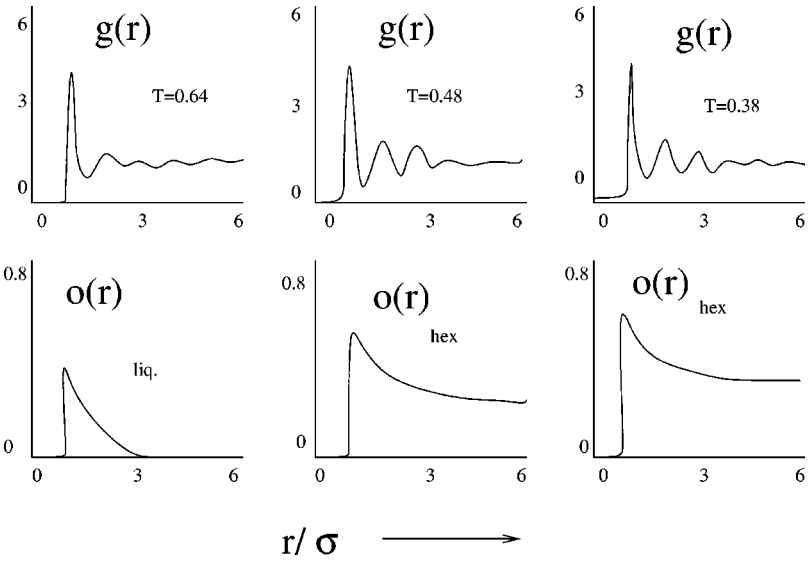

FIG. 22. Two-dimensional, in-plane positional correlation functions $[g(r)]$ and orientational correlation functions $[o(r)=\langle\Psi_6^*(0)\Psi_6(r)\rangle]$ for three different temperatures in the unwrapped contact layer shell. The plots are for LJ CCl_4 in a silica cylinder of diameter $12\sigma_{ff}$, showing the liquid and hexatic phases in the contact layer at $T^*=0.64$, $T^*=0.48$, and $T^*=0.38$.

TABLE II. Freezing temperatures: Molecular simulation.

H/σ_{ff}	k_BT/ϵ_{ff}	Ordered phase
$\geqslant$20 (large pores)	a	crystal
20	0.38	crystal
15	0.36	crystal+glass
12	0.34	hexatic+glass
9	0.34	hexatic+glass

[a]Gibbs–Thomson equation is valid.

V. CONCLUSION

Recently, the freezing behavior in slit shaped pores have been understood in considerable detail.[22] In the case of freezing in cylindrical geometry, the qualitative behavior is similar to that of slit-shaped pores. However, there are two important differences. First, the freezing temperatures in a cylindrical pore are in general lower than for a slit pore of the same porous material and pore size.[26] Second, a freezing transition is observed (resulting in a homogeneous crystalline confined phase) in the case of slit pores for all pore sizes down to the smallest pore size, that accommodates only one molecular layer of adsorbed molecules.[36,47] In the case of cylinders, however, our experiments as well as simulations clearly show that, a homogeneous crystalline confined phase results only for cylindrical pores with average diameters larger than $20\sigma_{ff}$. For cylindrical pores with diameters in the range $12<H/\sigma_{ff}<20$, the confined phase at low temperature is an inhomogeneous phase with partially crystalline domains interspersed with amorphous regions. For cylindrical pores with $H\leqslant 12\sigma_{ff}$, the confined phase at low temperature consists of a hexatic contact layer and an amorphous inner region.

Our simulations provide clear evidence of a contact layer hexatic phase that undergoes a hexatic to liquid transition at higher temperatures (the presence of a hexatic contact layer phase is established in the case of slit-shaped pores[36,59]). The experimental results also support this view. It is also clear from the simulations that the hexatic transition is a transition involving nearest neighbor bonds. In addition, for cylinders with diameters $H\geqslant 15\sigma_{ff}$, the contact layer hexatic phase undergoes a freezing transition as the temperature is lowered. For the case of the large cylinders, it is clear from our simulations that the freezing transition of the contact layer is different from the freezing transition in the inner layers. Thus, for a narrow range of temperatures, $T_{f,\text{inner region}}<T<T_{f,\text{contact layer}}$, the confined phase consists of crystalline contact layers with liquidlike inner region (the presence of such a frozen contact layer phase is very well established in strongly attractive slit-pores[22]). Although, it is not apparent from our experimental measurements that the contact layers freeze at a temperature different from the inner layers, some earlier experimental studies have reported ''prefreezing'' of the contact layer phase that results in a metastable phase characterized by crystalline contact layer and liquidlike inner region.[20,55] Theoretical justification of the metastable contact layer phase was provided by Sliwinska-Bartkowiak *et al.*, using Landau free energy surfaces.[20]

We have been careful in distinguishing between a crystalline phase and a glass phase in our simulations. Our choice of the bond orientational order parameter is helpful in this regard; unlike positional order parameters, such as $g(r)$ and $s(k)$, the bond orientational order parameters clearly distinguish a glass from a crsytal. The results of our simulations are reliable (we have calculated the free energy surface) for the finite system size we have studied. In the experiments, however, we only have indirect evidence of the nature of the confined phase based on the estimation of the rotational relaxation times of the molecules. Our interpretation of the experimental results is aided by the results of our simulation. The experimental results are consistent with the results of our simulations. Two obvious factors are not captured by our model: connectivity and surface heterogeneity. It is possible that both of these factors are going to affect the ordering in the confined phase, especially the subtle nature of the orientationally ordered hexatic contact layer. At this point it is unclear if either of these factors would completely destabilize (in a thermodynamic sense) the hexatic ordering in the contact layer. The experimental measurements seem to indicate otherwise.

Fluid molecules confined in cylindrical pores exhibit a rich phase behavior resulting in novel phases. It is therefore essential to study the structure of the confined phases using more direct experimental methods, such as x-ray diffraction and neutron scattering. Indirect experimental measurements using differential scanning calorimetry are insufficient to explore the rich phase-diagram of fluids confined in cylindrical nanopores. It is also important to extend the molecular simulations of confined phase freezing behavior to more realistic models of networked pore glasses[33] and MCM-41.

ACKNOWLEDGMENTS

It is a pleasure to thank Katsumi Kaneko and Kuni Morishige for helpful discussions. We are also grateful to Jolanta Gras for help with the DSC analysis involving nitrobenzene in MCM-41 and Vycor. R.R. thanks Adama Mickiewicz University, Poznan, Poland for their hospitality during a visit in the summer of 1999, when this work was carried out. This work was supported by grants from the National Science Foundation (Grant No. CTS-9896195) and KBN (Grant No. 2 PO3B 175 08), and by a grant from the U.S.–Poland Maria Sklodowska–Curie Joint fund (Grant No. MEN/DOE-97-314). Supercomputer time was provided under a NSF/NRAC Grant (MCA93S011).

[1] J. Warnock, D. D. Awschalom, and M. W. Shafer, Phys. Rev. Lett. **57**, 1753 (1986).
[2] J. L. Tell, H. J. Maris, and G. M. Seidel, Phys. Rev. B **28**, 5122 (1983).
[3] R. H. Torii, H. J. Maris, and G. M. Seidel, Phys. Rev. B **41**, 7167 (1990).
[4] P. E. Sokol *et al.*, Appl. Phys. Lett. **61**, 777 (1992).
[5] J. H. Strange, M. Rahman, and E. G. Smith, Phys. Rev. Lett. **71**, 3589 (1993).
[6] E. Molz, A. P. Y. Wong, M. H. W. Chan, and J. R. Beamish, Phys. Rev. B **48**, 5741 (1993).
[7] K. M. Unruh, T. E. Huber, and C. A. Huber, Phys. Rev. B **48**, 9021 (1993).
[8] J. A. Duffy, N. J. Wilkinson, H. M. Fretwell *et al.*, J. Phys.: Condens. Matter **7**, L713 (1995).
[9] E. W. Hansen, M. Stöker, and R. Schmidt, J. Phys. Chem. **100**, 2195 (1996).

[10] K. J. Elder, P. A. Reynolds, F. Trouw, and J. W. White, J. Chem. Soc. Chem. Commun. **1996**, 155.
[11] J. Krim, J. P. Coulomb, and J. Bouzidi, Phys. Rev. Lett. **58**, 583 (1987).
[12] K. Morishige and K. Nobuoka, J. Chem. Phys. **107**, 6965 (1997).
[13] K. Morishige and K. Kawano, J. Chem. Phys. **110**, 4867 (1998).
[14] K. Overloop and L. V. Gerven, J. Magn. Reson., Ser. A **101**, 179 (1993).
[15] H. F. Booth and J. H. Strange, Mol. Phys. **93**, 263 (1998).
[16] M. Sliwinska-Bartkowiak, J. Gras, R. Sikorski *et al.*, Langmuir **15**, 6060 (1999).
[17] R. Evans and U. Marini Bettolo Marconi, J. Chem. Phys. **86**, 7138 (1987).
[18] J. M. Baker, J. C. Dore, and P. Behrens, J. Phys. Chem. B **101**, 6226 (1997).
[19] S. Takahara, M. Nakano, S. Kittaka *et al.*, J. Phys. Chem. B **103**, 5814 (1999).
[20] M. Sliwinska-Bartkowiak, J. Gras, G. Dydziak *et al.*, in *Characterization of Porous Solids V*, edited by K. Unger, G. Kreysa, and J. Baselt (Elsevier, Amsterdam, 1999), p. 141.
[21] K. Morishige and K. Kawano, ''Dynamics in confinement,'' Workshop in Grenoble, January 2000.
[22] R. Radhakrishnan, K. Gubbins, and M. Sliwinska-Bartkowiak, J. Chem. Phys. **112**, 11048 (2000).
[23] K. Morishige and K. Kawano (preprint, 2000).
[24] D. W. Brown, P. E. Sokol, A. P. Clarke *et al.*, J. Phys.: Condens. Matter **9**, 7317 (1997); A. J. Brown, C. G. V. Burgess, D. H. Everett, and S. Nuttall, in *Characterization of Porous Solids IV*, edited by T. J. McEnaney *et al.* (Royal Society of Chemistry, Cambridge, 1997), pp. 1–8.
[25] M. Miyahara and K. E. Gubbins, J. Chem. Phys. **106**, 2865 (1997).
[26] M. Maddox and K. E. Gubbins, J. Chem. Phys. **107**, 9659 (1997).
[27] W. Haller, J. Chem. Phys. **42**, 686 (1965).
[28] T. Elmer, in *ASM Engineered Materials Handbook*, edited by S. Schnieder (ASM, Materials Park, Ohio, 1991), p. 427.
[29] I. Nowak and M. Ziolek, *Third Polish–German Zeolite Conference*, edited by M. Rozwadowski (Nicholas Copernicus University Press, Torun, 1998), p. 161.
[30] P. Debye, *Polar Molecules* (Chemical Catalog, New York, 1929).
[31] A. Chelkowski, *Dielectric Physics* (Elsevier, North–Holland, New York, 1980).
[32] B. K. Peterson, J. P. R. B. Walton, and K. E. Gubbins, J. Chem. Soc., Faraday Trans. 2 **82**, 1789 (1986).
[33] L. D. Gelb and K. E. Gubbins, Langmuir **14**, 2097 (1998).
[34] L. D. Landau and E. M. Lifshitz, *Statistical Physics*, 3rd ed. (Pergamon, London, 1980).
[35] G. Torrie and J. Valleau, Chem. Phys. Lett. **28**, 578 (1974).
[36] R. Radhakrishnan and K. E. Gubbins, Mol. Phys. **96**, 1249 (1999).
[37] J. S. Van Duijneveldt and D. Frenkel, J. Chem. Phys. **96**, 4655 (1992).
[38] R. M. Lynden-Bell, J. S. van Duijneveldt, and D. Frenkel, Mol. Phys. **80**, 801 (1993).
[39] P. Steinhardt, D. Nelson, and M. Ronchetti, Phys. Rev. B **28**, 784 (1983).
[40] C. G. Gray and K. E. Gubbins, *Theory of Molecular Fluids* (Clarendon, Oxford, 1984), Chap. 2 and Appendix A.
[41] K. Cole and R. Cole, J. Chem. Phys. **9**, 341 (1941).
[42] *Landolt–Börnstein Tables* (Springer-Verlag, Berlin, 1961).
[43] G. Bánhegyi, J. Colloid Interface Sci. **264**, 1030 (1986).
[44] P. Pissis, A. Kyritsis, D. Daoukaki *et al.*, J. Phys.: Condens. Matter **10**, 6025 (1998).
[45] J. Schüller, R. Richert, and E. Fischer, Phys. Rev. B **52**, 15232 (1995).
[46] M. Urbakh and J. Klafter, J. Phys. Chem. **97**, 3344 (1993).
[47] R. Radhakrishnan, K. Gubbins, A. Watanabe, and K. Kaneko, J. Chem. Phys. **111**, 9058 (1999).
[48] J. Brock, R. Birgeneau, J. Lister, and A. Aharony, Phys. Today **42**(7), 52 (1989).
[49] N. Mermin, Phys. Rev. **176**, 250 (1968).
[50] B. Halperin and D. Nelson, Phys. Rev. Lett. **41**, 121 (1978).
[51] D. Nelson and B. Halperin, Phys. Rev. B **19**, 2457 (1979).
[52] A. Young, Phys. Rev. B **19**, 1855 (1979).
[53] X. Zhao, G. Q. Lu, A. K. Whittaker, G. J. Millar, and H. Y. Zhu, J. Phys. Chem. B **101**, 6525 (1997).
[54] J. Klafter and J. Drake, *Molecular Dynamics in Restricted Geometries* (Wiley, New York, 1989).
[55] K. Morishige and K. Kawano, J. Phys. Chem. B (submitted).
[56] K. Morishige and K. Kawano, J. Chem. Phys. **112**, 11023 (2000).
[57] J. Kosterlitz and D. Thouless, J. Phys. C **5**, L124 (1972).
[58] J. Kosterlitz and D. Thouless, J. Phys. C **6**, 1181 (1973).
[59] R. Radhakrishnan, K. E. Gubbins, and M. Sliwinska-Bartkowiak, Phys. Rev. Lett. (submitted).